# PI3-kinase signaling contributes to orientation in shallow gradients and enhances speed in steep chemoattractant gradients

Bosgraaf, Leonard; Keizer-Gunnink, Ineke; van Haastert, Peter J. M.

*Published in:*
Journal of Cell Science

*DOI:*
10.1242/jcs.031781



*Publication date:*
2008

# PI3-kinase signaling contributes to orientation in shallow gradients and enhances speed in steep chemoattractant gradients

**Leonard Bosgraaf, Ineke Keizer-Gunnink and Peter J. M. Van Haastert***

Department of Molecular Cell Biology, University of Groningen, Kerklaan 30, 9751NN Haren, The Netherlands

*Author for correspondence (e-mail: P.J.M.van.Haastert@rug.nl)

*Accepted 4 August 2008*
*Journal of Cell Science 121, 3589-3597 Published by The Company of Biologists 2008*
*doi:10.1242/jcs.031781*

## Summary

***Dictyostelium*** **cells that chemotax towards cAMP produce phosphatidylinositol (3,4,5)-trisphosphate [PtdIns(3,4,5)$P_3$] at the leading edge, which has been implicated in actin reorganization and pseudopod extension. However, in the absence of PtdIns(3,4,5)$P_3$ signaling, cells will chemotax via alternative pathways. Here we examined the potential contribution of PtdIns(3,4,5)$P_3$ to chemotaxis of wild-type cells. The results show that steep cAMP gradients (larger than 10% concentration difference across the cell) induce strong PtdIns(3,4,5)$P_3$ patches at the leading edge, which has little effect on the orientation but strongly enhances the speed of the cell. Using a new sensitive method for PtdIns(3,4,5)$P_3$ detection that corrects for the volume of cytosol in pixels at the boundary of the cell, we show that, in shallow cAMP gradient (less than 5% concentration difference across the cell), PtdIns(3,4,5)$P_3$ is still somewhat enriched at the leading edge. Cells lacking PI3-kinase (PI3K) activity exhibit poor chemotaxis in these shallow gradients. Owing to the reduced speed and diminished orientation of the cells in steep and shallow gradients, respectively, cells lacking PtdIns(3,4,5)$P_3$ signaling require two- to six-fold longer times to reach a point source of chemoattractant compared with wild-type cells. These results show that, although PI3K signaling is dispensable for chemotaxis, it gives the wild type an advantage over mutant cells.**

Supplementary material available online at
http://jcs.biologists.org/cgi/content/full/121/21/3589/DC1

Key words: *Dictyostelium*, PI3-kinase, Chemotaxis

## Introduction

Chemotaxis is a vital process in a wide variety of organisms, ranging from bacteria to vertebrates (Baggiolini, 1998; Campbell and Butcher, 2000; Crone and Lee, 2002). Chemotaxis is achieved by coupling gradient sensing to basic cell movement. The difference in receptor occupation between each side of the cell leads to an internal polarization. A pseudopod is extended at the side with the highest receptor occupation while at the same time pseudopod formation at all other sides is repressed or existing pseudopodia are retracted, resulting in directional cell migration (Devreotes and Janetopoulos, 2003; Postma et al., 2004a).

It has been well documented that local areas of high phosphatidylinositol (3,4,5)-trisphosphate [PtdIns(3,4,5)$P_3$] concentrations [PtdIns(3,4,5)$P_3$ patches] are associated with increased concentrations of F-actin and pseudopod extension in neutrophils and *Dictyostelium* cells (Devreotes and Janetopoulos, 2003). PtdIns(3,4,5)$P_3$ is synthesized by PI3-kinases (PI3Ks) and degraded by 5-phosphatases such as SHIP and synaptojanin or by the 3-phosphatase tumor suppressor PTEN. In *Dictyostelium*, PtdIns(3,4,5)$P_3$ is degraded predominantly by PTEN (Iijima et al., 2004). Cells with a deletion of the *pten* gene show a substantial increase of PtdIns(3,4,5)$P_3$ levels, and a much broader leading edge both of PtdIns(3,4,5)$P_3$ patches and protrusions.

These very clear data have led to the convincing hypothesis that the local formation of PtdIns(3,4,5)$P_3$ at the side of the cell closest to the source of chemoattractant provides the directional information for chemotactic movement in *Dictyostelium* and mammalian cells (Ma et al., 2004; Merlot and Firtel, 2003; Parent et al., 1998). However, several observations suggest that this might not be the complete picture. The PI3K inhibitor LY29004 strongly inhibits cAMP-stimulated PtdIns(3,4,5)$P_3$ production, but has only minor effects on chemotaxis (Andrew and Insall, 2007; Chen et al., 2003; Funamoto et al., 2002; Loovers et al., 2006; Takeda et al., 2007). Furthermore, deletion of the genes encoding two cAMP-stimulated PI3Ks, which results in the near complete inhibition of detectable PtdIns(3,4,5)$P_3$ production (Huang et al., 2003), leads to only partial inhibition of chemotaxis in steep gradients (Funamoto et al., 2001; Loovers et al., 2006; Takeda et al., 2007). A study was recently conducted in which all five genes encoding recognizable type-I PI3Ks were disrupted, but cells still exhibited relatively good chemotaxis towards cAMP (Hoeller and Kay, 2007). However, movement of the PI3K mutants was not normal; they were slower and orientated poorly in weak gradients (Hoeller and Kay, 2007; Takeda et al., 2007). These data suggest that PtdIns(3,4,5)$P_3$ signaling is dispensable for chemotaxis in steep gradients, which leaves us with two important questions: what is/are the other pathway(s) that mediate chemotaxis in *pi3k*-null cells, and what is the contribution of PtdIns(3,4,5)$P_3$ to chemotaxis in wild-type cells? Recently, it was demonstrated that PLA2 and soluble guanylyl cyclase (sGC) partake in alternative pathways in *Dictyostelium*; inhibition of the PI3K, PLA2 or sGC pathway had small partial effects on chemotaxis, whereas simultaneous inhibition of all pathways nearly completely inhibited chemotaxis (Chen et al., 2007; van Haastert et al., 2007; Veltman et al., 2008). Other pathways, such as adenylyl cyclase, TORC2, PLC and $Ca^{2+}$ might also play

important roles in chemotaxis (Comer et al., 2005; Lee et al., 2005; Postma et al., 2004b; van Haastert et al., 2007).

We investigated the potential role of PtdIns(3,4,5)$P_3$ in the chemotaxis of wild-type cells. Several observations suggest that inhibition of PI3K reduces chemotaxis in shallow cAMP gradients, but not in steep gradients (Loovers et al., 2006; Takeda et al., 2007; van Haastert et al., 2007). We have been long confused by this observation because, in wild-type cells, strongly labeled patches of the PtdIns(3,4,5)$P_3$ detector, $PH_{CRAC}$-GFP, at the leading edge are detected in strong cAMP gradients, but not even weak $PH_{CRAC}$-GFP responses at the leading edge could be detected in shallow cAMP gradients, in which these wild-type cells exhibit excellent chemotaxis (presented here in Fig. 1B). Thus, how could PI3K mediate chemotaxis in shallow gradients if there is no PtdIns(3,4,5)$P_3$ formation detectable? We developed a novel method that discriminates better between $PH_{CRAC}$-GFP in the cytosol and at the boundary of the cell so that it has approximately tenfold higher sensitivity to detect PtdIns(3,4,5)$P_3$ responses then previous methods. Using this method, we show two types of $PH_{CRAC}$-GFP–PtdIns(3,4,5)$P_3$ responses: a small PtdIns(3,4,5)$P_3$ response in shallow cAMP gradients that is proportional to the gradient, and, as reported previously, a strong PtdIns(3,4,5)$P_3$ response in steep cAMP gradients. The PI3K inhibitor LY294002 inhibited both responses. Analysis of cell behavior in steep and shallow gradients with and without PI3K activity revealed that the strongly labeled PtdIns(3,4,5)$P_3$ patches are associated with an approximate twofold increase of the cell speed. The presence or absence of these PtdIns(3,4,5)$P_3$ patches had little effect on the strong chemotactic response in steep gradients. In shallow gradients, inhibition of PtdIns(3,4,5)$P_3$ signaling led to a strong reduction of chemotaxis. Overall, the contribution of PtdIns(3,4,5)$P_3$ signaling to directionality in shallow gradients and speed in steep gradients leads to a two- to six-fold faster migration towards a chemoattractant when compared with cells in which PtdIns(3,4,5)$P_3$ synthesis is blocked. Thus, although the PtdIns(3,4,5)$P_3$ signaling pathway is dispensable for chemotaxis in steep gradients, it plays an important role in chemotaxis and natural aggregation.

## Results

### Formation of $PH_{CRAC}$-GFP–PtdIns(3,4,5)$P_3$ patches in steep cAMP gradients

In order to investigate the function of PtdIns(3,4,5)$P_3$ in *Dictyostelium* chemotaxis, we made use of the established PtdIns(3,4,5)$P_3$-binding PH domain of CRAC, which was fused to GFP. Consistent with previous reports (Parent et al., 1998), we found that when cells were stimulated with a micropipette filled with 100 μM cAMP, they formed distinct regions towards the pipette that were highly enriched in $PH_{CRAC}$-GFP. Throughout this manuscript, these regions are termed patches. As explained later, we define a patch as a region at the cell boundary with an average GFP signal that is ≥1.5 times the mean fluorescence of the cytosol, has a minimum size of 2 μm and lasts for at least two consecutive frames (4-8 seconds/frame). These patches of $PH_{CRAC}$-GFP were observed in about 80% of the cells very close to the pipette (<20 μm), but were virtually absent in cells beyond a distance of 100 μm (Fig. 1A,B). Patch formation in 40% of the cells was observed at a distance of 50 μm. At this distance, the cAMP concentration was 200 nM and the absolute gradient was 2000 pM/μm (see Materials and Methods). Cells show a significant chemotactic response (threshold chemotaxis index=0.2) up to 1000 μm from a micropipette with 100 μM cAMP (Fig. 1B). At this distance, the cAMP concentration was 5 nM and the absolute gradient was 5 pM/μm. These findings suggest that $PH_{CRAC}$-GFP patches are formed only when the gradient of chemoattractant across the cell is above a certain threshold, approximately 1000 pM/μm.

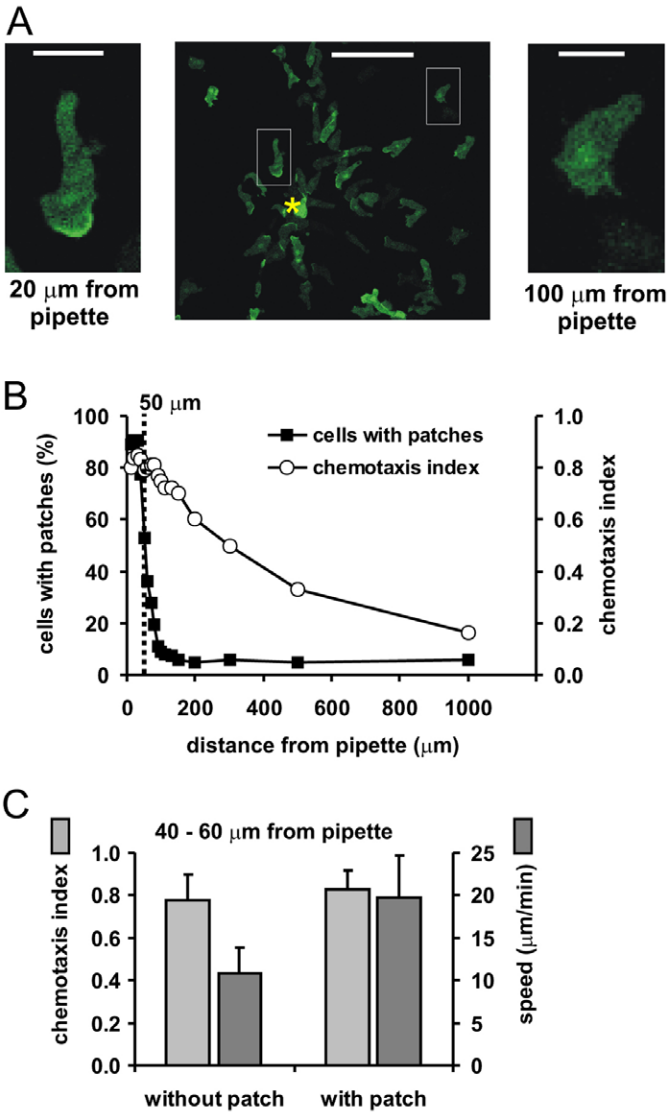


**Fig. 1.** Formation of $PH_{CRAC}$-GFP patches in steep cAMP gradients. Cells expressing $PH_{CRAC}$-GFP were stimulated with a micropipette filled with $10^{-4}$ M cAMP. (A) The confocal image reveals $PH_{CRAC}$-GFP patch formation at the leading edge of cells close to the pipette, but more uniform cytosolic localization of $PH_{CRAC}$-GFP in cells further away from the pipette. Two cells are shown at higher magnification. The asterisk indicates the position of the pipette. Scales bars: 50 μm (middle) and 10 μm (left and right). (B) The fraction of cells containing a $PH_{CRAC}$-GFP patch at the leading edge and the chemotaxis index were determined at different distances from the pipette. Half-maximal $PH_{CRAC}$-GFP patch formation occurs at a distance of about 50 μm from the pipette, and significant chemotaxis is observed up to 1000 μm from the pipette. (C) The chemotaxis index and speed of cells at 40-60 μm from the pipette was determined for 35 cells without and 22 cells with a $PH_{CRAC}$-GFP patch. Values are averages ± s.d.

### Role of PtdIns(3,4,5)$P_3$ patches in steep gradients

To deduce the function of $PH_{CRAC}$-GFP patches in steep gradients we determined several aspects of chemotaxis and cell movement at a distance of 40-60 μm from a pipette filled with 100 μM cAMP.

In this region, about 50% of the cells exhibited a $PH_{CRAC}$-GFP patch at the leading edge, whereas the other cells displayed a cytosolic distribution of $PH_{CRAC}$-GFP (Fig. 1A,B). These two groups of cells were exposed to the same cAMP gradient, and were in dynamic equilibrium because cells without a patch often obtained a patch somewhat later and vice versa. Quantitative analysis of the movement of the cells revealed that cells with a $PH_{CRAC}$-GFP patch essentially had the same chemotaxis index as cells without a $PH_{CRAC}$-GFP patch (Fig. 1C). By strong contrast, cells with a $PH_{CRAC}$-GFP patch exhibited a nearly twofold higher speed than cells without a $PH_{CRAC}$-GFP patch (Fig. 1C).

This twofold difference in speed matches our previous observation that pseudopodia that originate from $PH_{CRAC}$-GFP patches are two times larger than pseudopodia that were not initiated by a patch (Postma et al., 2004b). These findings strongly suggest that, in steep cAMP gradients, the $PH_{CRAC}$-GFP patches at the leading edge are responsible for the enhanced speed of the cells, but are not essential for chemotactic orientation. This conclusion is consistent with the observations that, in steep gradients, both *pi3k*-null cells and wild-type cells treated with the PI3K inhibitor LY294002 had the same chemotaxis index and speed as wild-type cells without $PH_{CRAC}$-GFP patches (see supplementary material Table S1).

### PI3K and chemotaxis in shallow cAMP gradients

To investigate the function of PtdIns(3,4,5)$P_3$ signaling in shallow cAMP gradients (below 1000 pM/μm), we performed three assays to measure the chemotaxis index and speed of control cells and cells with inhibited PI3K production (Fig. 2; supplementary material Table S1). Because LY294002 might not be completely specific and might inhibit pathways other than that of PI3K, the experiments were also performed with cells in which the *pi3k1* and *pi3k2* genes have been deleted (*pi3k*-null cells), which show a >90% reduction of the cAMP-induced PtdIns(3,4,5)$P_3$ accumulation (Funamoto et al., 2001; Huang et al., 2003). The data are in part identical to those published (Loovers et al., 2006), and were supplemented with additional data at other cAMP concentrations. The first experiment was performed by placing droplets containing cAMP next to droplets containing cells on an agar plate, revealing that inhibition of PI3K activity with LY294002 or by deletion of two *pi3k* genes leads to a reduction of chemotactic activity at low cAMP concentrations, but not at high cAMP concentrations (Fig. 2A). The second experiment was performed using a modified Zigmond chamber (Veltman and Van Haastert, 2006). We found that, under these conditions, the chemotaxis index was not affected by LY294002 when 1000 nM of cAMP was used in the source chamber, but was strongly inhibited at lower cAMP concentrations (Fig. 2B). Finally, the chemotaxis index of cells moving towards a micropipette filled with 100 μM cAMP was analyzed at different distances from the pipette. As shown in Fig. 2C, chemotaxis was hardly reduced in *pi3k*-null cells or by LY294002 in wild-type cells at short (<100 μm) distances, whereas further away from the pipette chemotaxis was increasingly inhibited. These findings suggest that, in shallow gradients, the PI3K pathway plays an important role in chemotaxis, consistent with previous observations (Loovers et al., 2006; Postma et al., 2004b; Takeda et al., 2007). Activation of the PI3K pathway is most probably required for cAMP production (Loovers et al., 2006): because cAMP relay may enhance the cAMP gradient far away from the pipette, the reduction of chemotaxis in cells with inhibited PI3K activity could be caused by the absence of cAMP relay. However, inhibition of cAMP relay using 2 mM caffeine has no effect on chemotactic activity (Brenner and Thoms, 1984) in steep or shallow gradients (P.J.M.V.H., unpublished observations), suggesting that cAMP relay does not play a crucial role in chemotaxis.

The input signal for chemotaxis is probably a spatial gradient of cAMP (Mato et al., 1975). Therefore, we expressed the chemotactic index obtained with these three assays as a function of the spatial gradient, which was calculated according to the equations presented in the Materials and Methods. Fig. 2D shows that the three assays

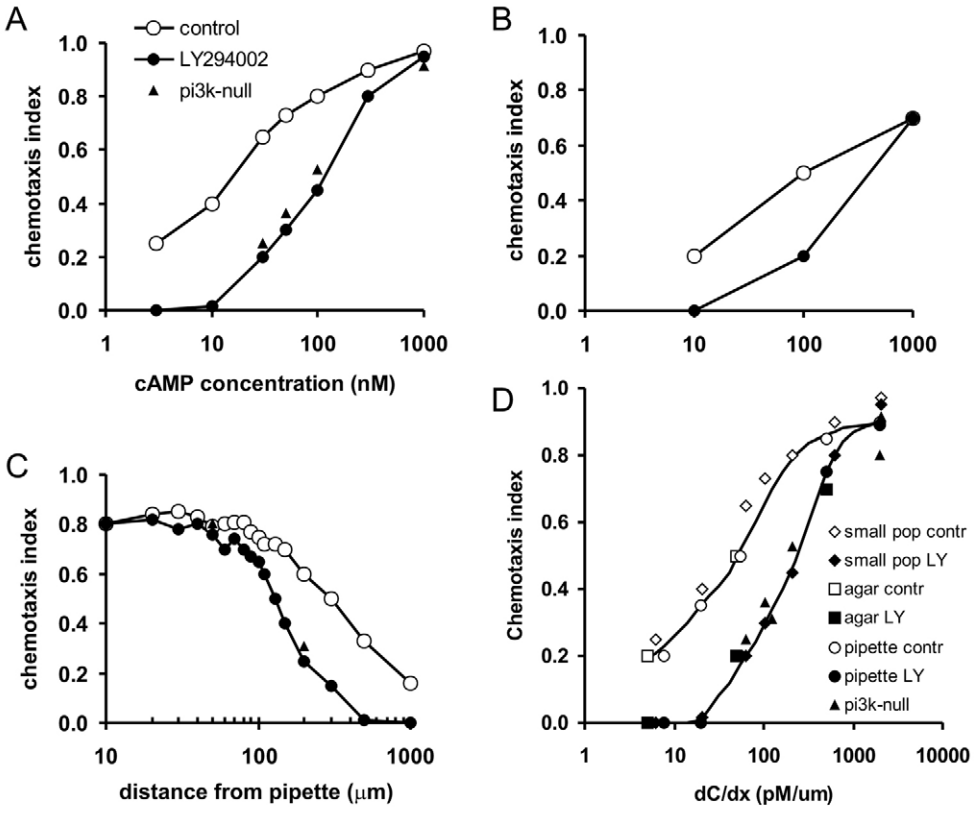


**Fig. 2.** Inhibition of PI3K signaling inhibits chemotaxis in shallow gradients but not in steep gradients. (A) Chemotactic activity was measured for *pi3k*-null cells and wild-type cells in the absence and presence of 50 μM LY294002 using (A) the small-population assay, (B) a Zigmond chamber or (C) the pipette assay. The cAMP gradients to which the cells are exposed were calculated using the equations presented in the Materials and Methods. (D) The chemotaxis index as function of the absolute gradient is shown. The data are the means of three experiments involving about 20 populations or cells analyzed in each experiment.

yielded essentially the same results, with half-maximal chemotaxis at a gradient of 50 pM/μm and threshold chemotaxis (CI=0.2) at ~6 pM/μm. Upon addition of LY294002 or by deletion of two genes encoding PI3Ks, the chemotaxis in shallow gradients was inhibited and the threshold for chemotaxis increased ~tenfold to 60 pM/μm. Furthermore, half-maximal chemotaxis was obtained at 225 pM/μm. In steeper gradients (above 750 pM/μm), the chemotaxis index was not affected by LY294002 or deletion of *pi3k* genes. These data suggest that PI3K inhibition leads to reduced chemotactic orientation in shallow gradients.

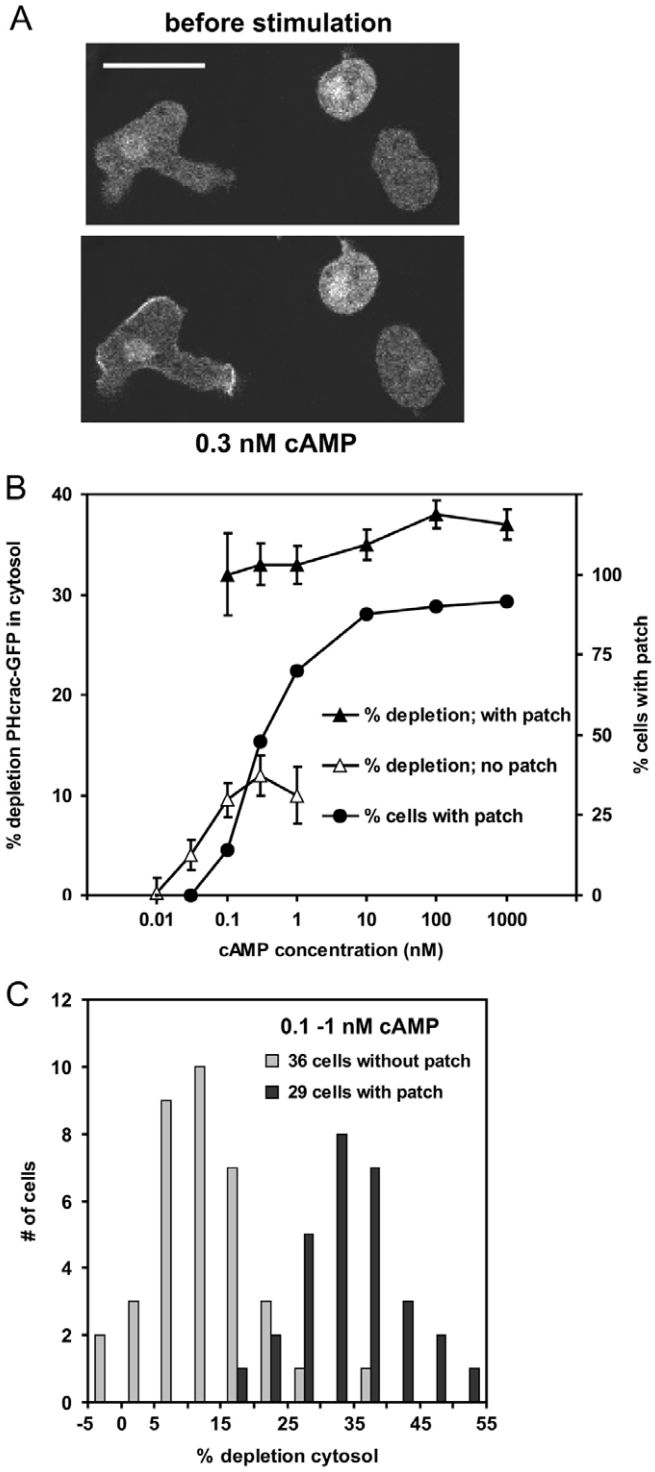


## $PH_{CRAC}$-GFP–PtdIns(3,4,5)$P_3$ localization

The above mentioned results strongly support a role for PtdIns(3,4,5)$P_3$ signaling in shallow gradients. However, we were not able to detect clear $PH_{CRAC}$-GFP patches at the leading edge in shallow cAMP gradients at distances beyond 100 μm from the pipette, i.e. below 500 pM/μm (Fig. 1A). As outlined below, assays detecting the redistribution of a GFP marker from the cytosol to the plasma membrane have a restricted sensitivity (see also Materials and Methods for more theoretical information). In confocal microscopy, fluorescence is typically detected in pixel elements with dimensions of 200×200×1000 nm (in x, y and z direction). A pixel element at the boundary of the cell will contain cytosol, plasma membrane and extracellular volume. We calculated that, for a *Dictyostelium* cell, approximately 70% of the pixels are interior and about 30% are at the boundary of the cell (see Materials and Methods). Assuming that, in unstimulated cells, all $PH_{CRAC}$-GFP is cytosolic, the boundary pixels will have an average fluorescence intensity that is half the fluorescence value of the interior pixels. When cAMP induces a significant but small (e.g. 10%) uniform translocation of $PH_{CRAC}$-GFP from the cytosol to the plasma membrane, this will lead to a decrease of the fluorescence intensity in the cytosol from 100% to 90%. The intensity of the boundary pixels will concurrently increase from 50% of the cytosol value to approximately 73%, which is still lower than the fluorescence intensity of the cytosol. Thus, the detection limit of translocation assays of a GFP-tagged protein from cytosol to membrane is poor when the increase at the membrane is measured. We used two assays to detect potential PtdIns(3,4,5)$P_3$ signaling at low cAMP concentrations. First, we studied depletion of fluorescence in the cytosol after stimulation with uniform cAMP concentrations, because accurate data can be obtained from the cytosol before and after uniform cAMP stimulation. Second, the increase of fluorescence at the boundary in cAMP gradients was measured, using a novel method to correct for the volume of the cytosol in each boundary pixel.

*Dictyostelium* cells stimulated with uniform cAMP exhibit a translocation of $PH_{CRAC}$-GFP to the membrane at very low cAMP concentrations (Loovers et al., 2006; Postma et al., 2004b). At 0.3 nM cAMP, approximately 45% of the cells showed strong patches of $PH_{CRAC}$-GFP at the membrane, whereas no detectable increase of $PH_{CRAC}$-GFP was detectable at the membrane of the other 55% of the cells (Fig. 3A).

Using the definition of patches (fluorescence intensity at the boundary at least 1.5-fold above the intensity in the cytosol, size above 2 μm and duration above 8 seconds), we discriminated

**Fig. 3.** Depletion of $PH_{CRAC}$-GFP from the cytosol after uniform stimulation with very low cAMP concentrations. Cells expressing $PH_{CRAC}$-GFP were stimulated in a perfusion chamber with the indicated concentration of cAMP. (A) Images before (top) and 14 seconds after (bottom) stimulation with 0.3 nM cAMP, showing one cell with $PH_{CRAC}$-GFP patches (left) and two cells with a more uniform cytosolic distribution of $PH_{CRAC}$-GFP (right). Scale bar: 10 μm. (B) Quantification of the decrease of fluorescence intensity of the cytosol after cAMP stimulation in cells with or without a $PH_{CRAC}$-GFP patch. The results show the means ± s.d. of 10 to 22 cells per cAMP concentration from two independent experiments. (C) Frequency distribution of the number of cells with different amounts of depletion of fluorescence intensity in the cytosol after stimulation with 0.1, 0.3 or 1 nM cAMP for cells with or without a $PH_{CRAC}$-GFP patch.

between cells containing a patch and cells that do not. For all 65 cells stimulated by 0.1 to 1 nM cAMP, the depletion of $PH_{CRAC}$-GFP in the cytosol was measured. The probability distribution for all cells is clearly bimodal, with a population of patch-containing cells showing a 33±7% reduction of the fluorescence intensity of the cytosol after cAMP stimulation (mean ± s.d., $n$=29), and a population of cells that does not contain a patch but still exhibits 12±7% ($n$=36) reduction of the fluorescence intensity of the cytosol. The fraction of cells containing depletions of around 20% is small, suggesting a biphasic response at increasing cAMP concentrations: at very low cAMP concentrations (<0.1 nM) a dose-dependent translocation of some $PH_{CRAC}$-GFP from the cytosol to plasma membrane occurs up to about 12% depletion in the cytosol; higher cAMP concentrations (>0.1 nM) lead to the enhanced depletion of 30% that is associated with the visible strong $PH_{CRAC}$-GFP patches at the membrane. We conclude that very low uniform cAMP concentrations can induce a significant PtdIns(3,4,5)$P_3$ response.

To increase the sensitivity of the assay for translocation of $PH_{CRAC}$-GFP to the membrane of cells in a cAMP gradient, we coexpressed $PH_{CRAC}$-GFP and the cytosol marker monomeric red fluorescent protein MARS (RFP), and simultaneously obtained confocal fluorescent images of both markers (Fischer et al., 2004). The fluorescence intensity of RFP provides information on the cytosolic volume of boundary pixels, which can then be used to calculate the membrane component of the $PH_{CRAC}$-GFP signal. For these calculations we first normalized the RFP signal to the average

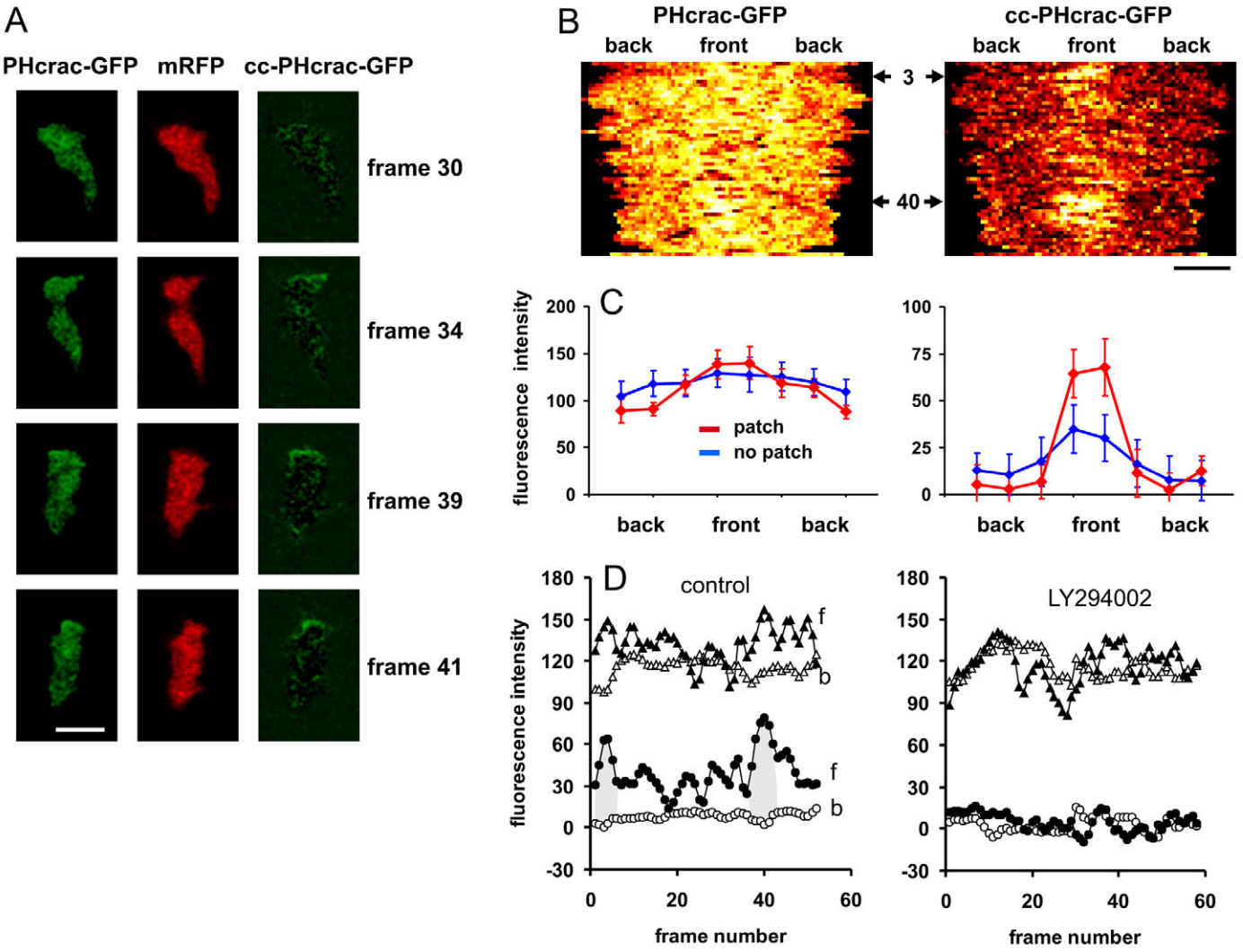


**Fig. 4.** Accumulation of $PH_{CRAC}$-GFP at the leading edge of cells stimulated with a gradient of cAMP. Cells expressing $PH_{CRAC}$-GFP and cytosolic mRFP were stimulated with a micropipette filled with 100 µM cAMP (see supplementary material Movie 1). (A) A typical cell at a distance of about 100 µm from the pipette is shown. The cell in frame 41 exhibits a faint $PH_{CRAC}$-GFP patch that is just visible in the confocal image of the GFP signal. The normalized mRFP signal of each pixel was subtracted from the GFP signal in that pixel to correct for the difference in cytosolic content of boundary pixel, yielding $ccPH_{CRAC}$-GFP. Scale bar: 10 µm. (B) The fluorescence intensity of $PH_{CRAC}$-GFP and $ccPH_{CRAC}$-GFP at the boundary of the cell for all frames is presented. For the $PH_{CRAC}$-GFP signal, a patch is visible around frames 3 and 40, but otherwise not many details can be recognized. In the panel showing $ccPH_{CRAC}$-GFP, not only these patches can be seen but nearly all frames show an increased fluorescence at the leading edge. (C) The fluorescence intensity at the boundary of the cell is quantified for the $PH_{CRAC}$-GFP and $ccPH_{CRAC}$-GFP signal. Data for a visible $PH_{CRAC}$-GFP patch are obtained from frames 3 or 4 and 39-42, and data for no visible $PH_{CRAC}$-GFP patch are obtained from the remaining frames. The data show the means ± s.d. (D) The fluorescence intensity at the boundary in the front (f, black symbols) or back (b, white symbols) of the cell for the $PH_{CRAC}$-GFP (triangles) and $ccPH_{CRAC}$-GFP (circles) signal is shown. The left panel in D is the same cell as is shown in A-C; the gray area indicates the strong patches. The right panel in D was of the same batch of cells after incubation with 50 µM LY294002.

GFP signal in that cell to correct for differences in expression levels between $PH_{CRAC}$-GFP and RFP. Then we subtracted the normalized RFP signal from the GFP signal in each pixel element, yielding cytosol-corrected $PH_{CRAC}$-GFP ($ccPH_{CRAC}$-GFP; see Materials and Methods for details). Images of the original $PH_{CRAC}$-GFP and $ccPH_{CRAC}$-GFP are presented in Fig. 4A for a cell that has a faint $PH_{CRAC}$-GFP patch at the membrane at around frame 3 and around frame 40; this cell is at a distance of about 100 μm from the pipette. In Fig. 4B, the fluorescence intensity in the boundary pixels is presented in space-time plots, whereas spatial data for frames with and without patches are presented in Fig. 4C, and temporal data for the front and back of the cell are shown in Fig. 4D. In the space-time plot of the $PH_{CRAC}$-GFP signal (Fig. 4B, left), the patches are just visible, but otherwise not much detail can be observed. After correction for the cytosol in boundary pixels, the $ccPH_{CRAC}$-GFP signal provides more details, with elevated fluorescence in the front region of the frames lacking obvious patches (Fig. 4B, right). The quantitative data reveal that the boundary $PH_{CRAC}$-GFP signal in the patch at the leading edge is about 139±12, compared with 95±12 at the side or back of the cell (all mean ± s.d.; $n$=4). The frames that do not contain a visible $PH_{CRAC}$-GFP patch also have no statistically significant difference in fluorescence intensity between the front and the side and/or back of the cell (125±9 versus 114±7). After correction for the cytosolic volume of boundary pixels, the $ccPH_{CRAC}$-GFP signal of patches was 66±3, compared with 6±5 at the side and/or back of the cell. More importantly, the frames that did not contain a visible $PH_{CRAC}$-GFP patch also exhibited significantly more fluorescence at the front (32±4) than at the side or in the back of the cell (9±4). Cells treated with the PI3K inhibitor LY294002 did not show a significantly different fluorescence intensity of $PH_{CRAC}$-GFP between the front and back of the cell, neither in the original data nor after cytosol correction (Fig. 4D).

The cell presented in Fig. 4 was located ~100 μm from the pipette and displayed clear but not very strong $PH_{CRAC}$-GFP patches. In a steep cAMP gradient at a distance of less than 50 μm from the pipette, strong $PH_{CRAC}$-GFP patches were observed with a typical $PH_{CRAC}$-GFP signal of 141±13 in the patch and 69±5 in the back of the cell, showing a ~twofold difference between the front and back of the cell, as has been observed before (Janetopoulos et al., 2004; Xu et al., 2005). After correction for the cytosol, the $ccPH_{CRAC}$-GFP values of this cell are 86±11 in the front and 2±4 at the side or back of the cell. The $ccPH_{CRAC}$-GFP fluorescence signal at the side or back of the cell was not significantly different from zero, which precludes the calculation of a ratio of $ccPH_{CRAC}$-GFP between the front and back of the cell. The data suggests that, in a steep cAMP gradient, the internal gradient of PtdIns(3,4,5)$P_3$ is much stronger than previously anticipated, and that the internal gradient of PtdIns(3,4,5)$P_3$ is also present in shallow cAMP gradients.

## Discussion

cAMP-stimulated cells exhibit two PtdIns(3,4,5)$P_3$ responses: a small gradual response in shallow gradients and a strong amplified response leading to a $PH_{CRAC}$-GFP patch in steep gradients. The small response is detectable when the depletion from the cytosol can be measured accurately (uniform stimulation) or when the response at the membrane can be corrected for the cytosol volume of boundary pixels (cAMP gradient). On the basis of these observations, we define a strong $PH_{CRAC}$-GFP patch as an area of the boundary of the cell with an uncorrected fluorescence intensity that is more than 1.5-fold higher than the fluorescence intensity of the cytosol; to exclude noise by individual pixels, patches should be larger than 2 μm and last for more than 8 seconds.

### The function of PI3K signaling in chemotaxis

We have shown here that inhibition of PI3K signaling with LY294002 or by deletion of two genes, encoding PI3K1 and PI3K2, leads to a significant inhibition of chemotaxis, but only in shallow gradients, in which the control cells have a chemotaxis index of less then ~0.5. In steeper gradients, in which control cells have a chemotaxis index above ~0.8, inhibition of PI3K signaling has far less effect on orientation of the cell.

Cell movement in buffer is best described as a random walk, i.e. cells extend a new pseudopod in a random direction every 30-60 seconds. In shallow gradients, new pseudopodia are still extended in all directions, but are either extended more frequently in the direction of the gradient than in other directions, or retracted less frequently. We suppose that activators and inhibitors regulate the time and place where a new pseudopod is made, and that stimulation of the cAMP receptor will influence the activity of one or multiple of these activators and inhibitors, thereby affecting pseudopod formation. In *Dictyostelium*, at least four signaling pathways have been implicated in chemotaxis: PI3K, PLA2, a soluble guanylyl cyclase protein (sGC) and cGMP produced by sGC (Veltman et al., 2008). Each of these chemoattractant-stimulated pathways may produce activators or inhibitors of pseudopodia. In a shallow gradient, in which the probability that a pseudopod is extended in the direction of the gradient is very low, interference with any of these hypothetical activators or inhibitors will lead to a reduction of chemotaxis. Therefore, inhibition of PI3K signaling will reduce chemotaxis in shallow gradients, even though three other parallel pathways are functional. In steep cAMP gradients, amplification of PI3K signaling leads to the formation of PtdIns(3,4,5)$P_3$ patches. These PtdIns(3,4,5)$P_3$ patches at the leading edge might help the cell in orienting towards the cAMP gradient, because actin-filament formation is stimulated in regions of the cytosol immediately below the membrane area with a PtdIns(3,4,5)$P_3$ patch (Funamoto et al., 2002; Parent et al., 1998; Postma et al., 2004b). However, we did not observed a difference of chemotaxis index between cells with or without $PH_{CRAC}$-GFP patches that were exposed to the same cAMP gradient. We propose that the PI3K pathway is dispensable for chemotaxis in steep gradients because the other PLA2, cGMP and sGC pathways provide sufficient orientation to yield a chemotaxis index of around 0.8.

In contrast to the absence of a strong effect of PI3K on orientation in steep gradients, we observed that cells with a $PH_{CRAC}$-GFP patch move towards the pipette about twofold faster than cells without $PH_{CRAC}$-GFP patches. In addition, we observed that, during uniform cAMP stimulation, pseudopodia extending from areas of the membrane with a $PH_{CRAC}$-GFP patch are about twofold larger than pseudopodia without $PH_{CRAC}$-GFP patches. These results suggest that membrane areas with PtdIns(3,4,5)$P_3$ patches induce extensive actin-filament formation, leading to large pseudopodia and fast forward movement of the cell.

The function of PI3K signaling in chemotaxis can be approached by proposing a ‘race’ between wild-type and *pi3k*-null cells towards a point source of chemoattractant. Using the measured speed and chemotaxis indices at different distances from the pipette, the time required by a cell to reach the pipette can be computed (Fig. 5; see Materials and Methods for equations). The *pi3k*-null cells are at a disadvantage because they have a lower chemotaxis index than wild-type cells far away from the pipette and move slower

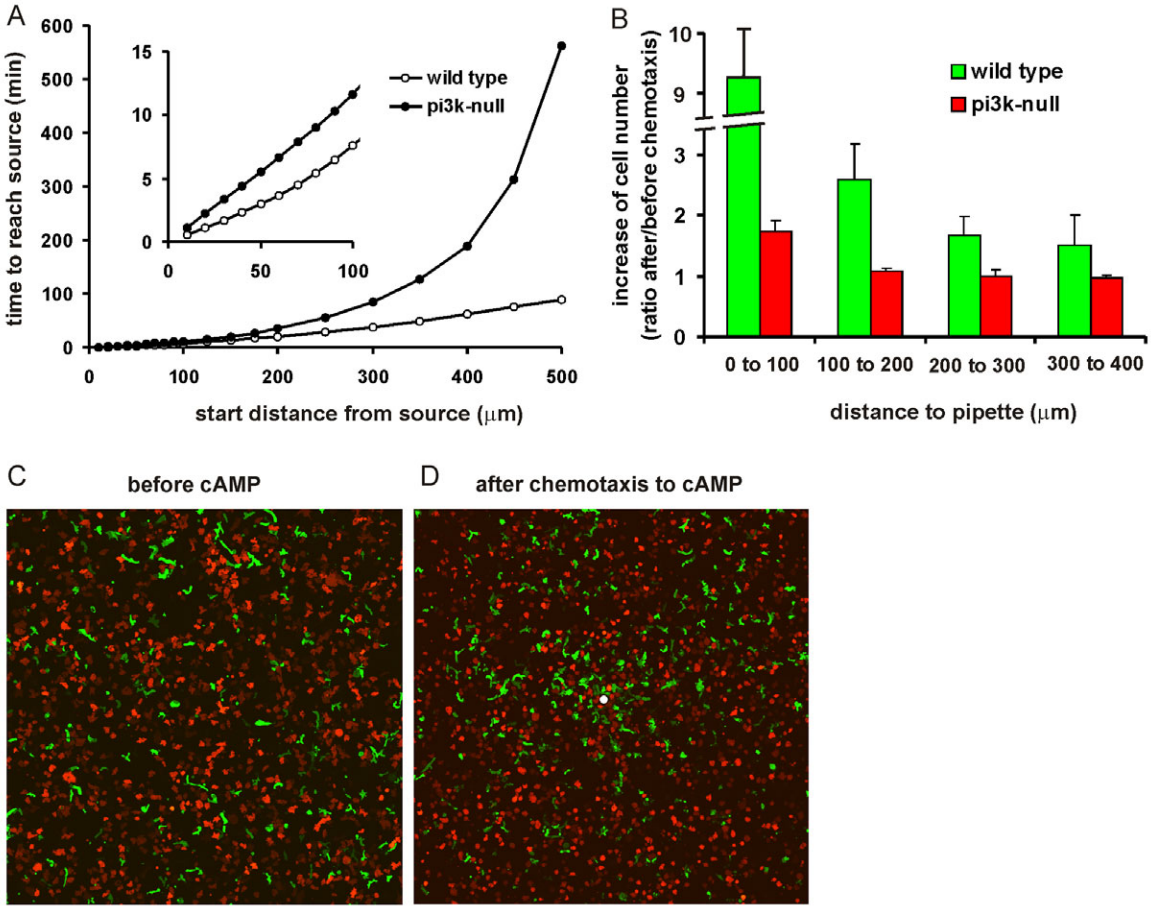


**Fig. 5.** Cells lacking PI3K activity are out competed by wild-type cells. (A) Calculations. The chemotaxis index and speed of the cells at different distances from a pipette containing 100 μM cAMP were determined for AX3 cells in the presence and absence of the PI3K inhibitor LY294002 (see Fig. 1C; Fig. 2; supplementary material Table S1). Using these data, the displacement in the direction of the pipette due to chemotaxis and random movement was calculated (see Materials and Methods for equations). Presented is the average time needed to reach the pipette from different starting positions. The data predict that PI3K-inhibited cells always arrive later at the source than wild-type cells and perform relatively well when starting from a distance of about 100 μm, but perform increasingly worse at larger distances from the source. (B-D) Experiment. Wild-type cells were transformed with a plasmid expressing cytosolic GFP, whereas *pi3k*-null cells were transformed with a plasmid expressing RFP. Cells were starved, mixed (wild-type:*pi3k*-null ratio is 1:3) and exposed to a cAMP gradient from a pipette containing 100 μM cAMP. Confocal images were recorded before (C) and 50 minutes after (D) application of the cAMP gradient. The white dot in the centre in D indicates the position of the pipette; the field of observation is 725×725 μm, recorded as 5×5 tile scans. The cell density was measured at different distances from the pipette before and after stimulation (B). The data show the increase of cell density as means ± s.d. of four determinations.

than wild-type cells close to the pipette. As a consequence, wild-type cells at a distance of 450 μm from the pipette are expected to reach the pipette in about 1 hour, whereas *pi3k*-null cells require 3 hours to tip the pipette. At longer distances from the pipette the situation is even worse, because *pi3k*-null cells do not exhibit chemotaxis beyond 450 μm. The cells must first reach this threshold distance by random movement before they can pick up the chemotactic signal, which requires about 30 hours when starting at a distance of 1000 μm. By contrast, wild-type cells exhibit significant chemotaxis at 1000 μm from the pipette, predicting that, in 4 hours, wild-type cells move from 1000 μm away to the pipette. Cells with inhibited PI3K activity perform optimally relative to wild-type cells when starting at a distance of about 100 μm from the pipette, a distance at which the chemotactic behavior of cells is usually determined. We have performed the race experiment by exposing a mixture of RFP-labeled *pi3k*-null cells and GFP-labeled wild-type cells to the same cAMP gradient. Before application of the cAMP gradient, the distribution of both cell types was approximately random (Fig. 5C). At 50 minutes after exposing cells to the cAMP gradient, many wild-type cells, but only a few *pi3k*-null cells, had moved close to the pipette (Fig. 5D). We determined the increase of cell density after application of the gradient as a function of the distance towards the pipette. The *pi3k*-null cells showed a modest 1.75-fold increase close to the pipette, and no increase beyond 100 to 200 μm from the pipette. By contrast, wild-type cells exhibit a nearly tenfold increase of cell density close to the pipette, and the density is still elevated at 400 μm from the pipette (Fig. 5B).

In summary, we have addressed three issues on the role of PI3K signaling in chemotaxis that were raised after it was observed that cells lacking PI3K signaling can exhibit excellent chemotaxis. First, parallel PLA2-sGC signaling pathways are responsible for chemotaxis in cells lacking PI3K activity. Second, two functions for PI3K signaling for chemotaxis were characterized, supporting orientation in shallow gradients and speed in steep gradients. Third, despite being dispensable, wild-type cells depend on PI3K signaling to effectively orient and move in a chemotactic gradient. In their natural habitat, cells use chemotaxis to trace bacteria for eating and

to form a multicellular structure for survival in the absence of food. In mixtures with wild-type cells, PI3K-deficient cells will be rapidly out competed.

## Materials and Methods

### Strain and culture conditions

The *pi3k*-null strain GMP1 has deletions of the *pi3k1* and *pi3k2* genes (Funamoto et al., 2001). A cell line expressing the PH domain of CRAC fused to GFP S65T (Parent et al., 1998) was made by electroporation of wild-type AX3 cells with plasmid WF38 (a generous gift of Peter Devreotes, Johns Hopkins University, MD). These $PH_{CRAC}$-GFP-expressing cells were selected and grown in HG5 medium with 10-40 μg/ml geneticin (Gibco) in dishes to 80% confluency. Cells were harvested and washed twice with 10 mM phosphate buffer, pH 6.5 (PB), and starved in a six-well plate (Nunc) at 80% confluency on 1% agarose in PB until the onset of aggregation.

### Definition of $PH_{CRAC}$-GFP patches

Cells in each frame of a movie were classified as 'cell with patch' or 'cell without patch'. We define a patch as a region at the cell boundary with an average GFP-signal that is ≥1.5 times the mean fluorescence of the cytosol and has a minimum size of 2 μm. To reduce the noise in the data, a patch must be present in at least two consecutive frames (4-8 seconds/frame). Conversely, when a patch disappears, it must be absent for at least two consecutive frames to identify the cell as a 'cell without patch'.

### Chemotaxis assays

Cells were harvested at the onset of aggregation, when dark-field waves become visible, and used for three chemotaxis assays. The small-population assay was performed as described (van Haastert et al., 2007). For the Zigmond-chamber assay (Zigmond, 1977), cells were deposited under the glass bridge of a modified Zigmond chemotaxis chamber (Veltman and Van Haastert, 2006). The bridge is ~2 mm wide and supported by two strips of 0.15-mm thickness. A block of agarose (1% w/v in PB) is placed at one side of the bridge and a block of agarose containing the indicated concentration of cAMP in PB is placed at the opposite side, making sure that both blocks make contact with the fluid under the bridge. A gradient is formed across the glass bridge by diffusion of the cAMP from the 'source' block to the 'sink' block. Cells were observed in an area of 100×100 μm at a distance of about 700 μm from the agar block containing cAMP.

A second chemotaxis assay using micropipettes filled with cAMP has often been used for *Dictyostelium* cells expressing $PH_{CRAC}$-GFP (Funamoto et al., 2001). Briefly, a droplet containing cells was deposited on a microscope slide. A micropipette containing 100 μM cAMP (femtotip, Eppendorf) was placed in the field of cells with a micromanipulator. cAMP was released from the pipette by diffusion. In some cases, a compensation pressure of 1 hPa was used. The formation of the cAMP gradient was deduced by measuring the release of the fluorescent dye lucifer yellow (molecular mass=457 Da) from the pipette. The fluorescence intensity at different distances from the pipette was recorded in pixel elements (0.404×0.404 μm) and calibrated using the fluorescence intensity of diluted lucifer yellow added homogeneously to the bath. In this work we report on chemotaxis in stable gradients, which are obtained in about 10 minutes in the Zigmond chamber, but nearly instantaneously in the micropipette assay (Marten Postma and P.J.M.V.H., unpublished).

The behavior of the cells was recorded using an inverted phase-contrast microscope equipped with a standard CCD camera (JVC TK-C1381), or a fluorescent confocal microscope (Zeiss LSM510) with a Plan-apochromat 63× magnification 1.40 NA oil-immersed objective. The fields of observation were 100×100 μm for the phase-contrast microscope and roughly 150×150 μm for the fluorescence confocal microscope. Images were taken every 4 to 8 seconds. The chemotaxis index, defined as the ratio of the cell displacement in the direction of the gradient and its total traveled distance, was determined as previously described (Veltman and Van Haastert, 2006). Briefly, the position of the centroid of a cell was determined with ImageJ at 30-second intervals. Using these coordinates, the chemotaxis index and speed of each 30-second step was calculated and averaged, yielding the chemotaxis index and speed of the cell. The data shown are the average and s.e.m. of the chemotaxis indices and speed from at least three independent experiments with about 25 cells per experiment.

### Cytosol correction of $PH_{CRAC}$-GFP in boundary pixels

Pixel elements at the boundary of the cell contain variable amounts of cytosol, which make a large contribution to the total fluorescence intensity of the boundary pixels (see below). When the amount of cytosol in these pixels could be measured, the fluorescence due to association of $PH_{CRAC}$-GFP with the membrane could be calculated, resulting in a significant increase of the sensitivity to detect PtdIns(3,4,5)$P_3$. To correct for the amount of cytosol in pixels at the boundary of the cell, the following approach was applied. Cells expressing $PH_{CRAC}$-GFP were transformed with plasmid pDM134, which contains a hygromycin-resistance cassette and the entire monomeric red fluorescent protein MARS open reading frame (Fischer et al., 2004), flanked by an actin-15 promoter and an actin-8 terminator. Cells were selected and grown in the presence of 10 μg/ml geneticin (Gibco) and 50 μg/ml hygromycin B (Invitrogen). Images of these $PH_{CRAC}$-GFP/RFP cells were recorded using the Zeiss 510 laser-scanning microscope using an argon (488 nm) and neon (543 nm) laser, respectively. The movies were imported to and processed with ImageJ. Processing involved subtraction of the average fluorescence of an area devoid of cells, followed by a 1-pixel smoothing step. Subsequently, the GFP/RFP normalization factor was determined for individual cells by manually selecting the interior of the cell (starting at ~1 μm from the cell boundary) and dividing the average fluorescence value of the GFP channel by the average RFP signal. This was repeated for five other frames throughout the movie, the average GFP:RFP ratio was calculated and the RFP channel was multiplied by this GFP:RFP ratio. Finally, the corrected RFP signal was subtracted from the GFP signal in the entire stack of pixel elements of the movie (see supplementary material Movie 1).

The resulting cc$PH_{CRAC}$-GFP movie was analyzed with a custom version of QuimP (Dormann et al., 2002). In brief, the membrane intensity was determined at circa 50 points around the cell by averaging the intensity of 3×3 pixels at those positions. The data were imported and further analyzed using Microsoft Excel.

### Equations used to calculate cAMP gradients

When a pipette filled with cAMP is inserted in a field of *Dictyostelium* cells, cAMP will diffuse continuously from the pipette, leading to a stable spatial gradient of which the concentration $C(x)$ and the spatial gradient $\nabla C(x)$ are dependent on the distance ($x$) from the pipette according to:

$$C(x) = \frac{\alpha C_p}{x} \quad (1)$$

and

$$\nabla C(x) = -\frac{\alpha C_p}{x^2}\ , \quad (2)$$

where $C_p$ is the cAMP concentration in the pipette and $\alpha$ is a proportionality constant that depends on the geometry of the pipette and the applied pressure. Using a fluorescent dye we determined experimentally that $\alpha$=0.05. These equations are both experimentally and theoretically accurate descriptions of the cAMP gradient at a distance beyond 15 μm from the pipette; at shorter distances, more-complex equations are required (Marten Postma and P.J.M.V.H., in preparation).

In the modified Zigmond chamber, cells are deposited under a bridge. A cAMP gradient is formed by placing agar blocks with buffer on one side of the bridge and an agar block with cAMP on the other side (Veltman and Van Haastert, 2006). After a while, cells experience a gradient with the following properties:

$$C(x) = C_s\left(1 - \frac{x}{L}\right), \quad (3)$$

and

$$\nabla C(x) = -\frac{C_s}{L}\ , \quad (4)$$

where $C_s$ is the cAMP concentration at the source, $x$ is the distance from the source (700 μm) and $L$ is the width of the bridge (2000 μm).

The small-population assay scores the chemotactic response of a population of cells towards a cAMP source that has been applied at some distance away as a single dose. Owing to diffusion in the agar, a transient cAMP gradient is formed that is maximal with the following properties (Mato et al., 1975):

$$C(x) = 0.48\frac{r^3}{x^3}C_d \quad (5)$$

and

$$\nabla C(x) = 2.42\frac{r^3}{x^4}C_d\ , \quad (6)$$

where $r$ is the radius of the cAMP droplet (150 μm), $x$ is the distance between cell population and cAMP source (250 μm), and $C_d$ is the applied cAMP concentration in the droplet.

### Threshold for observing translocation of the cytosolic marker to the membrane

We are interested in the amount of depletion of $PH_{CRAC}$-GFP from the cytosol that leads to a significant increase of the fluorescence intensity at the membrane above the level of the cytosol. A confocal image of a cell is composed of internal pixel elements and boundary pixel elements. The pixel elements have dimensions of 400×400×1000 nm in the x, y and z direction, respectively, with a volume of 0.16 $\mu m^3$. The fluorescence intensity of an internal pixel element is $I_c$, and the average fluorescence intensity in the boundary pixel element is $I_b$. The boundary pixel elements consist of extracellular, intracellular and membrane volume. The membrane has a thickness of about 5 nm, which implies a volume of the membrane in a boundary pixel element that is maximally $1.4\times400\times1000\times5=0.28\times10^{-3}$ $\mu m^3$, or 0.175% of

the pixel volume. Therefore, the volume of the average boundary pixel consists of nearly 50% extracellular and 50% intracellular medium. The fluorescence intensity of the boundary pixel element is thus $I_b=I_m+0.5I_c$, where $I_m$ is the fluorescence intensity associated with the plasma membrane. Assume that the total number of pixel elements is $n$ and the fraction of boundary pixel elements is $a$.

Assume that, before cAMP stimulation, all $PH_{CRAC}$-GFP is localized in the cytosol, then $I_c=I_c^0$, and $I_b=0.5\,I_c^0$. Assume that, after cAMP stimulation, the fraction $g$ of the $PH_{CRAC}$-GFP in the cytosol translocates to the membrane. Then the fluorescence intensity after stimulation in the interior pixels is $I_c^s=(1–g)I_c^0$ and in the boundary pixels is $I_b^s=ga^{-1}I_c^0+(0.5–g)I_c^0$.

We are interested in the condition at which the fluorescence intensity of the boundary pixels surpasses the fluorescence intensity of the interior pixels, i.e. $I_b/I_c>1$. The ratio of fluorescence intensity at the boundary and interior pixels is given by:

$$I_b/I_c = [ga^{-1}I_c^0+(0.5–g)I_c^0]/(1–g)I_c^0 = [(g/a)+0.5–g]/(1–g)\ . \quad (7)$$

The fraction of pixel elements at the boundary (a) depends on the size of the pixels, and the size and shape of the cell. For a spherical cell with radius of 5 μm and pixel elements as indicated above, we estimate $a$=0.24, and for an elongated cell with length of 15 μm and radius 4 μm we estimate $a$=0.30. Using three-dimensional reconstruction of a cell expressing a transmembrane protein membrane, we observed $a$=0.26.

Supplementary material Fig. S1 shows that, for $a$=0.25, the fluorescence intensity of the boundary pixel elements becomes higher than the fluorescence intensity of the cytosol ($I_b/I_c>1$) when the depletion in the cytosol is above 12%. Thus, cAMP-induced translocations of $PH_{CRAC}$-GFP smaller than 12% cannot be easily detected at the boundary of the cell. This threshold for detecting translocation to the membrane will be smaller (i.e. more easily detected) when pixels elements are smaller, because the number of interior and boundary pixel elements increase with the power of three and two, respectively, by which the fraction of boundary pixels ($a$) decreases.

## Equations used to calculate cell movement in cAMP gradients

A cell at time $t$ and position $x$ from the pipette has a speed of $v(x,t)$ and chemotaxis index of $CI(x,t)$. The distance $\Delta A(x,t)$ moved towards the pipette at that position during a time interval $\Delta t$ is given by:

$$\Delta A(x,t) = \Delta\vec{A}(x,t) + \Delta\breve{A}(x,t) = v(x,t)CI(x,t)\Delta t + \sqrt{v(x,t)\Delta t}\ , \quad (8)$$

where $\Delta\vec{A}(x,t)=v(x,t)CI(x,t)\Delta t$ is the distance moved towards the pipette due to chemotaxis and $\Delta\breve{A}(x,t)=\sqrt{v(x,t)\Delta t}$ is the distance moved in the direction of the pipette due to random movement.

The distance moved after a large time period $t$ is given by:

$$A(x,t) = \sum_{t=0}^{t=t} v(x,t)CI(x,t)\Delta t + \sqrt{v(x,t)t}\ . \quad (9)$$

This equation was numerically solved for different start positions $x_s$ to obtain $A(x,t)=A(x_s,t_s)$, i.e. the time $t_s$ to reach the source of chemoattractant.

The chemotaxis index $CI(x)$ at distance ($x$) from the pipette was calculated from the spatial gradient (see above) and the fitted chemotaxis index at different spatial gradients obtained, as shown in Fig. 2D:

$$\Delta C = \alpha C_p / x^2$$

and

$$CI(x) = CI_{MAX}\frac{\Delta C^n}{\Delta C^n + K^n}\ , \quad (10)$$

where $\alpha$=0.05, $C_p=10^8$ pM, $CI_{MAX}$=0.9, $K$=26 pM/μm and $n$=0.9 for wild-type cells, and $K$=166.5 pM/μm and $n$=1.28 for *pi3k*-defective cells.

The speed $v(x)$ at distance ($x$) from the pipette is given by:

$$v(x) = v_0 + (v_p - v_0)F(x),$$

where $v_0$ and $v_p$ are the speed of cells without and with patch, respectively, obtained from supplementary material Table S1, and $F(x)$ is the fraction of cells with a patch from Fig. 1B (the fitted curve is:

$$F(x) = \sigma\frac{\beta}{x+\beta}\ ,$$

where σ is the maximal fraction of PtdIns(3,4,5)$P_3$ patches, and β is the distance at which half-maximal patches are observed; σ=0.8 and β=50 μm). Calculations were performed with $v_0$=10 μm/minute for both wild-type and *pi3k*-defective cells, and $v_p$=19 μm/minute for wild-type cells with a patch.

## References


**Andrew, N. and Insall, R. H.** (2007). Chemotaxis in shallow gradients is mediated independently of PtdIns 3-kinase by biased choices between random protrusions. *Nat. Cell Biol.* **9**, 193-200.

**Baggiolini, M.** (1998). Chemokines and leukocyte traffic. *Nature* **392**, 565-568.

**Brenner, M. and Thoms, S. D.** (1984). Caffeine blocks activation of cyclic AMP synthesis in Dictyostelium discoideum. *Dev. Biol.* **101**, 136-146.

**Campbell, J. J. and Butcher, E. C.** (2000). Chemokines in tissue-specific and microenvironment-specific lymphocyte homing. *Curr. Opin. Immunol.* **12**, 336-341.

**Chen, L., Janetopoulos, C., Huang, Y. E., Iijima, M., Borleis, J. and Devreotes, P. N.** (2003). Two phases of actin polymerization display different dependencies on PI(3,4,5)P3 accumulation and have unique roles during chemotaxis. *Mol. Biol. Cell* **14**, 5028-5037.

**Chen, L., Iijima, M., Tang, M., Landree, M. A., Huang, Y. E., Xiong, Y., Iglesias, P. A. and Devreotes, P. N.** (2007). PLA(2) and PI3K/PTEN pathways act in parallel to mediate chemotaxis. *Dev. Cell* **12**, 603-614.

**Comer, F. I., Lippincott, C. K., Masbad, J. J. and Parent, C. A.** (2005). The PI3K-mediated activation of CRAC independently regulates adenylyl cyclase activation and chemotaxis. *Curr. Biol.* **15**, 134-139.

**Crone, S. A. and Lee, K. F.** (2002). The bound leading the bound: target-derived receptors act as guidance cues. *Neuron* **36**, 333-335.

**Devreotes, P. and Janetopoulos, C.** (2003). Eukaryotic chemotaxis: distinctions between directional sensing and polarization. *J. Biol. Chem.* **278**, 20445-20448.

**Dormann, D., Libotte, T., Weijer, C. J. and Bretschneider, T.** (2002). Simultaneous quantification of cell motility and protein-membrane-association using active contours. *Cell Motil. Cytoskeleton* **52**, 221-230.

**Fischer, M., Haase, I., Simmeth, E., Gerisch, G. and Muller-Taubenberger, A.** (2004). A brilliant monomeric red fluorescent protein to visualize cytoskeleton dynamics in Dictyostelium. *FEBS Lett.* **577**, 227-232.

**Funamoto, S., Milan, K., Meili, R. and Firtel, R. A.** (2001). Role of phosphatidylinositol 3′ kinase and a downstream pleckstrin homology domain-containing protein in controlling chemotaxis in dictyostelium. *J. Cell Biol.* **153**, 795-810.

**Funamoto, S., Meili, R., Lee, S., Parry, L. and Firtel, R. A.** (2002). Spatial and temporal regulation of 3-phosphoinositides by PI 3-kinase and PTEN mediates chemotaxis. *Cell* **109**, 611-623.

**Hoeller, O. and Kay, R.** (2007). Chemotaxis in the absence of PIP3 gradients. *Curr. Biol.* **17**, 813-817.

**Huang, Y. E., Iijima, M., Parent, C. A., Funamoto, S., Firtel, R. A. and Devreotes, P.** (2003). Receptor-mediated regulation of PI3Ks confines PI(3,4,5)P3 to the leading edge of chemotaxing cells. *Mol. Biol. Cell* **14**, 1913-1922.

**Iijima, M., Huang, Y. E., Luo, H. R., Vazquez, F. and Devreotes, P. N.** (2004). Novel mechanism of PTEN regulation by its phosphatidylinositol 4,5-bisphosphate binding motif is critical for chemotaxis. *J. Biol. Chem.* **279**, 16606-16613.

**Janetopoulos, C., Ma, L., Devreotes, P. N. and Iglesias, P. A.** (2004). Chemoattractant-induced phosphatidylinositol 3,4,5-trisphosphate accumulation is spatially amplified and adapts, independent of the actin cytoskeleton. *Proc. Natl. Acad. Sci. USA* **101**, 8951-8956.

**Lee, S., Comer, F. I., Sasaki, A., McLeod, I. X., Duong, Y., Okumura, K., Yates, J. R., 3rd, Parent, C. A. and Firtel, R. A.** (2005). TOR complex 2 integrates cell movement during chemotaxis and signal relay in Dictyostelium. *Mol. Biol. Cell* **16**, 4572-4583.

**Loovers, H. M., Postma, M., Keizer-Gunnink, I., Huang, Y. E., Devreotes, P. N. and van Haastert, P. J.** (2006). Distinct roles of PI(3,4,5)P3 during chemoattractant signaling in Dictyostelium: a quantitative in vivo analysis by inhibition of PI3-kinase. *Mol. Biol. Cell* **17**, 1503-1513.

**Ma, L., Janetopoulos, C., Yang, L., Devreotes, P. N. and Iglesias, P. A.** (2004). Two complementary, local excitation, global inhibition mechanisms acting in parallel can explain the chemoattractant-induced regulation of PI(3,4,5)P3 response in dictyostelium cells. *Biophys. J.* **87**, 3764-3774.

**Mato, J. M., Losada, A., Nanjundiah, V. and Konijn, T. M.** (1975). Signal input for a chemotactic response in the cellular slime mold Dictyostelium discoideum. *Proc. Natl. Acad. Sci. USA* **72**, 4991-4993.

**Merlot, S. and Firtel, R. A.** (2003). Leading the way: directional sensing through phosphatidylinositol 3-kinase and other signaling pathways. *J. Cell Sci.* **116**, 3471-3478.

**Parent, C. A., Blacklock, B. J., Froehlich, W. M., Murphy, D. B. and Devreotes, P. N.** (1998). G protein signaling events are activated at the leading edge of chemotactic cells. *Cell* **95**, 81-91.

**Postma, M., Bosgraaf, L., Loovers, H. M. and Van Haastert, P. J.** (2004a). Chemotaxis: signalling modules join hands at front and tail. *EMBO Rep.* **5**, 35-40.

**Postma, M., Roelofs, J., Goedhart, J., Loovers, H. M., Visser, A. J. and Van Haastert, P. J.** (2004b). Sensitization of Dictyostelium chemotaxis by phosphoinositide-3-kinase-mediated self-organizing signalling patches. *J. Cell Sci.* **117**, 2925-2935.

**Takeda, K., Sasaki, A. T., Ha, H., Seung, H. A. and Firtel, R. A.** (2007). Role of phosphatidylinositol 3-kinases in chemotaxis in Dictyostelium. *J. Biol. Chem.* **282**, 11874-11884.

**van Haastert, P. J. M., Keizer-Gunnink, I. and Kortholt, A.** (2007). Essential role of PI 3-kinase and phospholipase A2 in Dictyostelium chemotaxis. *J. Cell Biol.* **177**, 809-816.

**Veltman, D. M. and Van Haastert, P. J.** (2006). Guanylyl cyclase protein and cGMP product independently control front and back of chemotaxing Dictyostelium cells. *Mol. Biol. Cell* **17**, 3921-3929.

**Veltman, D. M., Keizer-Gunnink, I. and Van Haastert, P. J. M.** (2008). Four key signaling pathways mediating chemotaxis in *Dictyostelium discoideum*. *J. Cell Biol.* **180**, 747-753.

**Xu, X., Meier-Schellersheim, M., Jiao, X., Nelson, L. E. and Jin, T.** (2005). Quantitative imaging of single live cells reveals spatiotemporal dynamics of multistep signaling events of chemoattractant gradient sensing in Dictyostelium. *Mol. Biol. Cell* **16**, 676-688.

**Zigmond, S. H.** (1977). Ability of polymorphonuclear leukocytes to orient in gradients of chemotactic factors. *J. Cell Biol.* **75**, 606-616.